Commun Nonlinear Sci Numer Simulat 89 (2020) 105284

Contents lists available at ScienceDirect

Commun Nonlinear Sci Numer Simulat

journal homepage: www.elsevier.com/locate/cnsns

Research paper

Modulation instability, rogue waves and spectral analysis for the sixth-order nonlinear Schrödinger equation

Yunfei Yue[a], Lili Huang[a,b], Yong Chen[a,c,d,*]

[a] School of Mathematical Sciences, Shanghai Key Laboratory of PMMP East China Normal University, Shanghai, 200062, China
[b] College of Mathematics and Statistics, Chongqing University, Chongqing, 401331, China
[c] College of Mathematics and Systems Science, Shandong University of Science and Technology, Qingdao, 266590, China
[d] Department of Physics, Zhejiang Normal University, Jinhua, 321004, China

ARTICLE INFO

Article history:
Received 18 January 2019
Revised 25 January 2020
Accepted 5 April 2020
Available online 7 May 2020

Keywords:
Nonlinear Schrödinger equation
Modulation instability
Rogue wave
Darboux transformation

ABSTRACT

Modulation instability, rogue waves and spectral analysis are investigated for the nonlinear Schrödinger equation with the higher-order terms. The modulation instability distribution characteristics from the sixth-order to eighth-order nonlinear Schrödinger equations are studied. Higher-order dispersion terms are closely related to the distribution of modulation stability regime, and n-order dispersion term corresponds to $n-2$ modulation stability curves in the modulation instability band. Based on the generalized Darboux transformation method, the higher-order rational solutions are constructed. Then the compact algebraic expression of the N-order rogue wave is given. Dynamic phenomena of the first- to third-order rogue waves are illustrated, which exhibit meaningful structures. Two arbitrary parameters play important roles in the rogue wave solution. One parameter can control the width and crest deflection of rogue wave, while the other can cause the change of width and amplitude of rogue wave. When it comes to the third-order rogue wave, three typical nonlinear wave structures, including fundamental, circular and triangular patterns, are displayed and discussed. Through spectral analysis on the first-order rogue wave, when these parameters satisfy certain conditions, it occurs a transition between W-shaped soliton and rogue wave.

1. Introduction

It has been extensive interests in studying rogue waves in recent years. Rogue wave was first put forward conceptually in the ocean [1]. Rogue waves are relatively large and spontaneous waves, whose appearance may result in catastrophic damage [2]. Large amplitude, unexpected, coming out from nowhere without warning and suddenly vanishing away without trace, are the basic characteristics [3]. The generation of rogue waves is closely related to modulation instability (MI). In optical communication system, the interplay between the dispersion and nonlinear effects can result into MI, which is an universal and very important physical phenomenon. The research on MI is conducive to improving the performance of optical communication system. Following the groundbreaking hydrodynamics work of Benjamin and Feir in the early 1960s [4], MI has played a prominent role in diverse areas of scientific research, for example, plasma physics [5], nonlinear optics [6], and fluid dynamics [7].

* Corresponding author.
E-mail address: ychen@sei.ecnu.edu.cn (Y. Chen).

https://doi.org/10.1016/j.cnsns.2020.105284
1007-5704/

In fact, the above mentioned instability can result in self-induced modulation of incoming continuous waves with subsequent local pulses, which may be discovered in many physical systems. Due to the presence of this phenomenon, there are many interesting physical effects, such as break-up of deep water-gravity waves in the ocean, the formation of envelope solitons in electrical transmission lines and optical fibers, as well as the formation of cavitons in plasmas. Different distributions of the MI gain can lead to distinct patterns of nonlinear dynamic phenomena [8]. The dispersion term and the nonlinear term play different roles in the nonlinear systems, but both of them affect the stability of the solutions for the nonlinear systems. Recently, some literatures have analyzed the importance of the higher-order dispersion terms, which is not only affect the MI [9] but also induce some novel excited states [10,11]. The study of MI regions in nonlinear systems is crucial in many fields, and is the basis for interpreting various models or natural phenomena.

The nonlinear Schrödinger (NLS henceforth) equation has a prominent position in nonlinear physics. It has extensive physical applications, especially in nonlinear optics [12], atmosphere [13], and water waves [14]. In 1983, Peregrine [15] gave the analytical expression of rogue wave in the first-order, as a result of MI on the constant wave background. This type of rogue wave also has another name, that is Peregrine breather. In recent years, many authors [16–18] have reported the higher-order rogue wave solutions of the NLS equation. In addition, various extensions of the NLS equation have also been studied, such as pair-transition-coupled NLS equation [19], variable coefficient NLS equation [20–22], three-component NLS equations[23], three-component coupled derivative NLS equations [24], and n-component NLS equations [25]. General higher-order solitons of three different types of nonlocal NLS equations in the reverse-time, PT-symmetric and reverse-space-time were derived by using a Riemann-Hilbert treatment [26].

However, there exists only the lowest-order dispersion and nonlinearity terms in the standard NLS equation [27]. When the characteristics of the solutions exceed the simple approximation in deriving the NLS equation, the higher-order terms will hold the dominate role [28]. For instance, it may help to illustrate the physics of wave blow-up and collapse phenomena [29]. Recently, there has been a series of outstanding and meaningful work on the higher-order NLS hierarchy [30–32]. Kedziora et al. [30] presented the infinite NLS hierarchy with time variable coefficients and the integrability of the whole hierarchy with each independent higher-order operator. Chowdury et al. [31] investigated the dynamics of MI when the higher-order terms preserve the integrability of the infinite NLS hierarchy. In 2016, Ankiewicz *et al*[32]. studied different nonlinear waves of the NLS equation with higher-order nonlinear and dispersion terms in the following form

$$iq_z + \delta_2\Gamma_2(q) - i\delta_3\Gamma_3(q) + \delta_4\Gamma_4(q) - i\delta_5\Gamma_5(q) + \delta_6\Gamma_6(q) - i\delta_7\Gamma_7(q) + \delta_8\Gamma_8(q) + \cdots = 0, \tag{1}$$

with

$$\begin{aligned}
\Gamma_2 &= q_{tt} + 2q|q|^2,\\
\Gamma_3 &= q_{ttt} + 6q^2 q_t,\\
\Gamma_4 &= q_{tttt} + 6q^* q_t^2 + 4q|q_t|^2 + 8|q|^2 q_{tt} + 2q^2 q_{tt}^* + 6|q|^4 q,\\
\Gamma_5 &= q_{ttttt} + 10|q|^2 q_{ttt} + 30|q|^4 q_t + 10q q_t q_{tt}^* + 10q q_t^* q_{tt} + 20q^* q_t q_{tt} + 10q_t^2 q_t^*,\\
\Gamma_6 &= q_{tttttt} + q^2[60|q_t|^2 q^* + 50q_{tt}(q^*)^2 + 2q_{tttt}^*] + q[12q^* q_{tttt} + 18q_t^* q_{ttt} + 8q_t q_{ttt}^* + 70(q^*)^2 q_t^2 + 22|q_{tt}|^2]\\
&\quad + 10q_t[3q^* q_{ttt} + 5q_t^* q_{tt} + 2q_t q_{tt}^*] + 10q^3[2q^* q_{tt}^* + (q_t^*)^2] + 20q^* q_{tt}^2 + 20q|q|^6,\\
\Gamma_7 &= q_{ttttttt} + 70q_{tt}^2 q_t^* + 112q_t|q_{tt}|^2 + 98|q_t|^2 q_{ttt} + 70q^2\{q_t[2q^* q_{tt}^* + (q_t^*)^2] + q^*(2q_{tt} q_t^* + q_{ttt} q^*)\}\\
&\quad + 28q_t^2 q_{ttt}^* + 14q[q^*(20|q_t|^2 q_t + q_{ttttt}) + 3q_{ttt} q_{tt}^* + 2q_{tt} q_{ttt}^* + 2q_{tttt} q_t^* + q_t + q_{tttt}^* + 20q_t q_{tt}(q^*)^2]\\
&\quad + 140|q|^6 q_t + 70q_t^3(q^*)^2 + 14(5q_{tt} q_{ttt} + 3q_t q_{tttt})q^*,\\
\Gamma_8 &= q_{tttttttt} + 14q^3[40|q_t|^2(q^*)^2 + 20(q^*)^3 q_{tt} + 2q^* q_{tttt}^* + 4q_t^* q_{ttt}^* + 3(q_{tt}^*)^2]\\
&\quad + q^2[28q^*(14|q_{tt}|^2 + 6q_t q_{ttt}^* + 11q_t^* q_{ttt} + 238q_{tt}(q_t^*)^2 + 336|q_t|^2 q_{tt}^* + 560q_t^2(q^*)^3\\
&\quad + 98q_{tttt}(q^*)^2 + 2q_{tttttt}^*] + 2q\{21q_t^2[9(q^*)^2 + 14q^* q_{tt}^*] + q_t[728q_{tt} q_t^* q^* + 238q_{ttt}(q^*)^2\\
&\quad + 6q_{ttttt}^*] + 34|q_{ttt}|^2 + 36q_{tttt} q_{tt}^* + 22q_{tt} q_{tttt}^* + 20q_{ttttt} q_t^* + 161q_{tt}^2(q^*)^2 + 8q_{tttttt} q^*\}\\
&\quad + 182q_{tt}|q_{tt}|^2 + 308q_{tt} q_{ttt} q_t^* + 252q_t q_{ttt} q_{tt}^* + 196q_t q_{tt} q_{ttt}^* + 168q_t q_{tttt} q_t^* + 42q_t^2 q_{tttt}^*\\
&\quad + 14q^*(30q_t^3 q_t^* + 4q_{ttttt} q_t + 5q_{ttt}^2 + 8q_{tt} q_{tttt}) + 490(q^*)^2 q_t^2 q_{tt} + 140q^4 q^*[q^* q_{tt}^* + (q_t^*)^2] + 70q|q|^8,
\end{aligned}$$

where $|q| = |q(z, t)|$ denotes envelope of the optical pulse with spatial coordinate z and scaled time coordinate t, δ_i ($i = 2, 3, 4, 5, \cdots\infty$) represents the i-order real dispersion coefficient. Γ_3 is the Hirota operator [33], Γ_4 is the Lakshmanan-Porsezian-Daniel operator [34], Γ_5 is known as the quintic operator [35], Γ_6 is the sextic operator, Γ_7 is the heptic operator, Γ_8 is the octic operator. With an infinite number of arbitrary coefficients, these extensions are integrable. The arbitrariness of coefficients enables us to go well beyond the single NLS equation.

The motivation of this paper is to generalize the distribution law of MI for the NLS equation with higher-order terms and analyze the influence of different parameters on rogue wave, then through the research of the sixth-order NLS equation to verify whether the results are consistent with MI from the spectrum analysis and consider under what conditions rogue wave can be transformed into W-shaped soliton. First of all, MI of a continuous wave for the NLS Eq. (1) with different higher-order terms is investigated. We will discuss MI distribution characteristics from the sixth-order NLS equation to the eighth-order NLS equation. Comparing their MI gain functions of NLS equations with different order dispersion terms, it enables us to find the distribution law of MS curves in the MI band.

Nowadays many methods have been developed to investigate rogue waves of the nonlinear systems, such as the Darboux transformation (DT) [36–42], Hirota method [43–46], nonlocal symmetry method [47]. Based on the generalized DT [36], higher-order rogue waves will be constructed for the following sixth-order NLS equation [48–50] with only the higher-order dispersion term

$$iq_z + \delta_2\Gamma_2(q) + \delta_6\Gamma_6(q) = 0, \tag{2}$$

which can be used to describe the pulses propagating along an optical fiber [48,50]. In [48], bilinear forms and soliton solutions of the generalized sixth-order NLS equation were derived by the Hirota method. In [49], breather to soliton transitions for the sixth-order NLS equation were investigated by the DT method. In [50], multi-soliton solutions of the sixth-order NLS equation were derived by the Hirota method. Here we will consider the plane wave solution of (2) containing space variable z and time variable t in studying MI and rogue wave solution. For the parameter δ_2, many papers [51–53] have chosen $\delta_2 = \frac{1}{2}$, this setting has certain convenient features. Here, we also set $\delta_2 = \frac{1}{2}$ in Eq. (2).

Via the analytical rational expressions and MI characteristics, the dynamics of rogue waves will be studied in detail. Then we investigate how to use the spectral features of the propagating wave envelope to reveal the existence of nonlinearity and rogue wave in a short time before the occurrence of a special rogue wave event [54]. For this purpose, we apply the spectral analysis approach [55–58] to the first-order rogue wave solution of Eq. (2).

The remainder of our article is constructed as follows. In Section 2, MI distribution features of the NLS equation with different higher-order nonlinear and dispersion terms will be discussed according to MI analysis theory. By virtue of the generalized DT, a concrete expression of the N-order rogue wave solutions for the sixth-order NLS equation will be given in Section 3. In Section 4, Utilizing the formulas obtained in the previous section, the first-order, second-order, and third-order exact rogue wave solutions are presented, where their dynamic behavior are also analyzed. Section 5 is devoted to spectral analysis on the first-order rogue wave. Finally, some conclusions are given.

2. Modulation instability

MI is observed in a time-averaged way and usually triggered from a continuous wave or quasi-continuous wave. The continuous wave condition is corresponding to an effectively unbounded MI domain. Then it can yield information on average behavior of the nonlinear process and the general tendencies for instability, but usually prevents time-resolved of the stochastic dynamics. MI symmetry breaking can occur for the reason of higher-order dispersion [59]. MI is the basic mechanism for generating rogue wave solutions. MI is an interactive gain procedure that generates priority frequency intervals between patterns [60]. Studied here is the MI analysis on continuous waves for the NLS equation with different higher-order dispersion terms, in order to reveal the MI features arising from the higher-order dispersion effects. The plane wave solution of system (1) has the following form

$$q_{\mathrm{cw}} = Ae^{i\theta} = Ae^{i(kz+\omega t)}. \tag{3}$$

Substituting Eq. (3) into Eq. (2), it can be obtained that

$$k = 20A^6\delta_6 - 90A^4\omega^2\delta_6 + 30A^2\omega^4\delta_6 - \omega^6\delta_6 + A^2 - \frac{1}{2}\omega^2, \tag{4}$$

which is the wave number of the plane wave. The background frequency is ω, and the amplitude is A. According to the MI theory, we add a small perturbation function $p(z, t)$ to the plane wave solution. Then a perturbation solution can be derived as

$$q_{\mathrm{pert}} = (A + \epsilon p(z,t))e^{i(kz+\omega t)}, \tag{5}$$

where $p(z,t) = me^{i(Kz+\Omega t)} + ne^{-i(Kz+\Omega t)}$, Ω indicates the disturbance frequency, and m, n are both small parameters. Substituting the perturbation solution (5) into the sixth-order NLS Eq. (2), it can generate a system of linear homogeneous equations for m and n. Based on the existence conditions for solutions of linear homogeneous equations, that is, the determinant of the coefficient matrix for the system of m and n is equal to 0, it gives rise to the following dispersion relation equation

$$\begin{aligned}
&4K^2 + (16\Omega\omega\delta_6(90A^4 - (30\Omega^2 + 60\omega^2)A^2 + 3\Omega^4 + 10\omega^2\Omega^2 + 3\omega^4) + 8\Omega\omega)K\\
&+ 4\Omega^2\delta_6^2(3600A^{10} + (-3300\Omega^2 + 10800\omega^2)A^8 + (1240\Omega^4 - 5400\omega^2\Omega^2 - 7200\omega^4)A^6\\
&+ (-240\Omega^6 + 1140\omega^2\Omega^4 + 600\omega^4\Omega^2 + 5760\omega^6)A^4 + (24\Omega^8 - 120\omega^2\Omega^6 + 180\omega^4\Omega^4 - 1020\omega^6\Omega^2\\
&- 540\omega^8)A^2 - \Omega^{10} + 6\Omega^8\omega^2 - 15\Omega^6\omega^4 + 22\Omega^4\omega^6 + 15\Omega^2\omega^8 + 36\omega^{10}) + 4\Omega^2\delta_6(120A^6 - 70A^4\Omega^2\\
&+ (14\Omega^4 + 30\omega^2\Omega^2 - 180\omega^4)A^2 - \Omega^6 - 3\omega^2\Omega^4 + 25\omega^4\Omega^2 + 12\omega^6) + \Omega^2(4A^2 - \Omega^2 + 4\omega^2) = 0.
\end{aligned}$$

By solving this dispersion relation equation, MI gain can be obtained

$$\begin{aligned}
G_6 &= |Im(K)| = \frac{1}{2}Im\left(|\Omega|\sqrt{(\Omega^2 - 4A^2)g_6^2}\right),\\
g_6 &= 1 + \left[2\Omega^4 + (-20A^2 + 30\omega^2)\Omega^2 + 60A^4 - 180A^2\omega^2 + 30\omega^4\right]\delta_6.
\end{aligned} \tag{6}$$

When $\Omega^2 - 4A^2 < 0$, the wave number K will exist the imaginary part which makes the perturbation function p exponentially increase and destroys the stability of the system. This instability is a condition for the existence of rogue wave. Moreover, It can be seen from the gain G_6 that the parameters Ω, ω, A, δ_6 play a pivotal role in MI of the sixth-order NLS system. If setting $\delta_6 = 0$, the gain G_6 will reduce to the standard NLS equation case.

Similar to the above calculation process, we also obtain the MI gain functions of the seventh-order (i.e. $\delta_2 = \frac{1}{2}, \delta_7 \neq 0, \delta_3 \cdots \delta_6 = 0$ in Eq. (1)) and eighth-order (i.e. $\delta_2 = \frac{1}{2}, \delta_8 \neq 0, \delta_3 \cdots \delta_7 = 0$ in Eq. (1)) NLS equations, respectively. Their exact expressions are as follows

$$\begin{aligned} G_7 &= |Im(K)| = \frac{1}{2} Im\left(|\Omega|\sqrt{(\Omega^2 - 4A^2)g_7^2}\right), \\ g_7 &= 1 + \left[14\,\omega\,\Omega^4 + \left(-140A^2\omega + 70\,\omega^3\right)\Omega^2 + 420A^4\omega - 420A^2\omega^3 + 42\,\omega^5\right]\delta_7, \end{aligned} \tag{7}$$

and

$$\begin{aligned} G_8 &= |Im(K)| = \frac{1}{2} Im\left(|\Omega|\sqrt{\left(\Omega^2 - 4A^2\right)g_8^2}\right), \\ g_8 &= 1 + \Big[-2\,\Omega^6 + \left(28A^2 - 56\,\omega^2\right)\Omega^4 + \left(-140A^4 + 560A^2\omega^2 - 140\,\omega^4\right)\Omega^2 \\ &\quad + 280A^6 - 1680A^4\omega^2 + 840A^2\omega^4 - 56\,\omega^6\Big]\delta_8. \end{aligned} \tag{8}$$

Let δ_7 and δ_8 be 0, then gain G_7 and G_8 can also reduce to the standard NLS equation case. For Eqs. 6–(8), the gain $G_i (i = 6, 7, 8)$ increases with the corresponding polynomial g_i under the condition $|\Omega| < 2A$.

From the above analysis, it appears that there exists two distinctive MI and modulation stability (MS) regions, which are distinguished with each other clearly. In the region $|\Omega| < 2A$, MI exists when $g_i \neq 0, (i = 6, 7, 8)$. On the contrary, if $g_i = 0, (i = 6, 7, 8)$, there appears nontrivial features in the MI region. This in turn implies that a MS region occurs in the region of low perturbation frequency, where the growth rate of corresponding MI decays to zero.

Comparing their MI gain functions of NLS equations with different order dispersion terms, we can obtain the distribution law of MS curves in the MI band, see Fig. 1.

- When $\delta_2 = \frac{1}{2}$ and the remaining coefficients $\delta_i = 0, i = 3, 4, 5, \cdots$, the system (1) can reduce to the classical NLS equation. And the highest power of $g_2(\omega)$ is equal to 0, namely, $g_2(\omega) = 1$. Therefore, no MS region exists in the MI band ($|\Omega| < 2A$), which is described in Fig. 1(a).
- When $\delta_2 = \frac{1}{2}$ and the other coefficients only $\delta_3 \neq 0$, the system (1) is transformed into third-order NLS equation. And the highest power of $g_3(\omega)$ is 1, i.e. a simple factor of ω. It appears that an MS curve exists in the MI band ($|\Omega| < 2A$), which is described in Fig. 1(b). When $\delta_3 = -0.1$, it can get the MI feature of the Hirota equation in [62].
- When $\delta_2 = \frac{1}{2}$ and the other coefficients only $\delta_4 \neq 0$, the system (1) can be degenerated to fourth-order NLS equation. The highest power of $g_4(\omega)$ is 2. There exists an MS elliptic ring in the MI band ($|\Omega| < 2A$), see Fig. 1(c). Here we consider the standard NLS equation with only the fourth-order term and the MI map is similar to the result in [63], where the third-order term $i\delta_3\Gamma_3(q)$ and the fourth-order term $\delta_4\Gamma_4(q)$ are considered.
- When $\delta_2 = \frac{1}{2}$ and the other coefficients only $\delta_5 \neq 0$, we can transform (1) into fifth-order NLS equation. The highest power of $g_5(\omega)$ is 3. Both an MS curve and an MS quasi-elliptic ring occur in the MI band ($|\Omega| < 2A$), which is illustrated in Fig. 1(d).
- When $\delta_2 = \frac{1}{2}$ and the other coefficients only $\delta_6 \neq 0$, we can transform (1) into sixth-order NLS equation. And the highest power of $g_6(\omega)$ is 4. There are two MS quasi-elliptic rings in the MI band ($|\Omega| < 2A$), see Fig. 1(e).
- When $\delta_2 = \frac{1}{2}$ and the other coefficients only $\delta_7 \neq 0$, Eq. (1) is reduced to seventh-order NLS equation. The highest power of $g_7(\omega)$ is 5. There exists an MS curve and two MS quasi-elliptic rings in the MI band ($|\Omega| < 2A$), see Fig. 1(f).
- When $\delta_2 = \frac{1}{2}$ and the other coefficients only $\delta_8 \neq 0$, we can transform (1) into eighth-order NLS equation. And the highest power of $g_8(\omega)$ is 6. Then it reveals that two MS curves and two MS quasi-elliptic rings exist in the MI band ($|\Omega| < 2A$). The distribution of this case is illustrated in Fig. 1(g).

The MI distribution features of all above higher-order dispersion NLS equations are illustrated in Fig. 1. According to the above analysis, it is evident that there exist two arbitrary parameters, namely higher order dispersion coefficient $\delta_i, i = 2, 3, 4 \cdots$ and amplitude A. These parameters control the MS distribution of system (1) in the MI band. By adjusting the parameters, the MS quasi-elliptic and MS elliptic ring can be completely contained within the MI band or intersected at the MI boundary, the latter case yields two curves in the MI band. Fig. 1 only shows one case that the MS ellipse is contained in the MI band when the semi-major axis of the MS ellipse less than 2. When choosing appropriate values of parameters to make the semi-major axis of the MS ellipse greater than 2, we can get another case that only the MS curves exist in the MI band. From Fig. 1(g), there appears that the MS elliptic ring in the middle degenerates into two MS curves.

By analyzing the expressions in Eq. (6), we can discuss the MI distribution characteristics of the sixth-order NLS Eq. (2). Obviously, g_6 is a polynomial about ω and its highest power is 4. If this polynomial factor is decomposed into the product form of single factors, then we can get four solutions, which means that G_6 has four curves in the frequency plane (ω, Ω). Here, Fig. 1(e) illustrates the MI gain distribution features in the frequency plane (ω, Ω). It is clear that this frequency plane

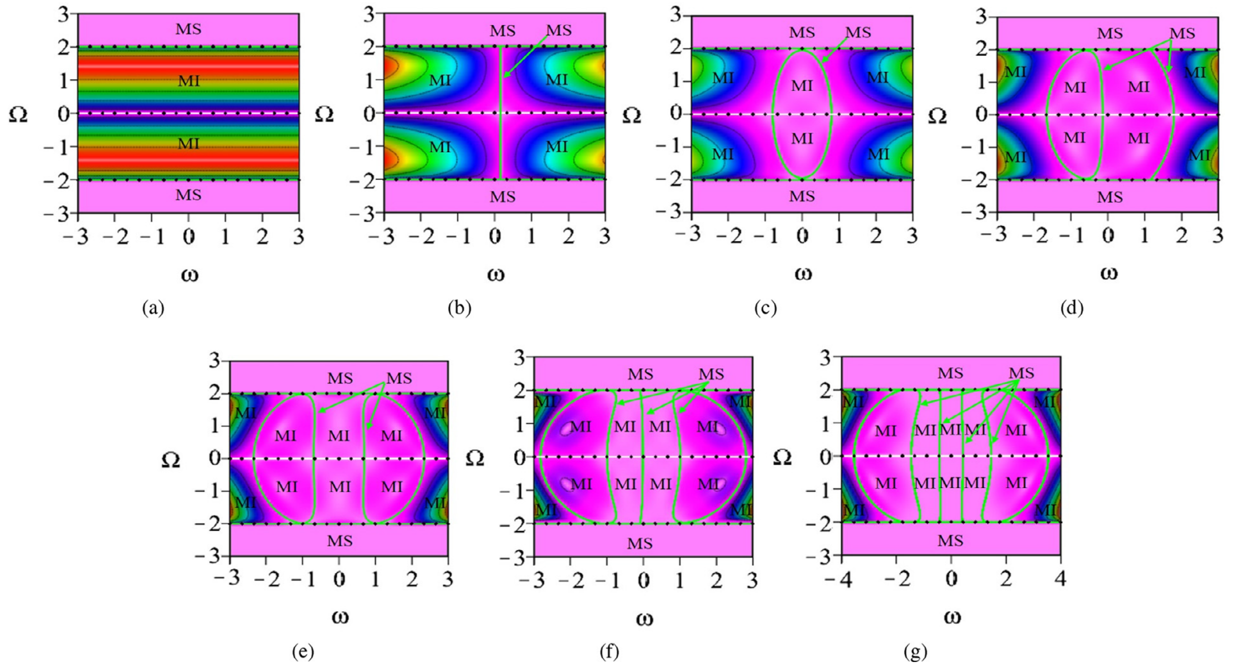

Fig. 1. Plots of the distribution of MI gain with perturbation frequency Ω and continuous background frequency ω, and $A = 1$. The dashed white lines indicate the resonance lines, the dashed green lines mean boundary lines, and the solid green lines represent that perturbation is stable. In addition to MS curves and MS quasi-elliptic curves, the remaining areas are all non-zero MI gain in the MI band. (a) The standard NLS equation [61] with $\delta_2 = 1/2$: no MS region exists in the MI band. (b) The Hirota equation [62] with $\delta_3 = 1$: an MS curve exists in the MI band. (c) The Lakshmanan-Porsezian-Daniel equation [63] with $\delta_4 = -(7+\sqrt{15})/48$: an MS elliptic ring appears in the MI band. (d) The fifth-order NLS equation [64,65] with $\delta_5 = 0.12$: it has not only an MS curve, but also an MI quasi-elliptic ring in the MI band. (e) The sixth-order NLS equation with $\delta_6 = 0.05$: it has two MS quasi-elliptic rings in the MI band. (f) The seventh-order NLS equation with $\delta_7 = 0.2$: an MS curve and two MS quasi-elliptic rings in the MI band. (g) The eighth-order NLS equation with $\delta_8 = 0.1$: two MS curves and two MS quasi-elliptic rings appear in the MI band. (For interpretation of the references to color in this figure legend, the reader is referred to the web version of this article.)

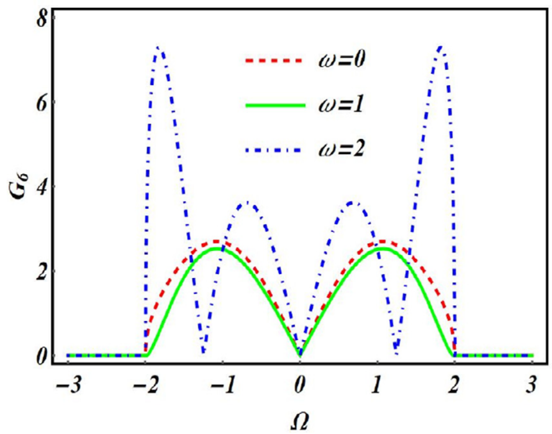

Fig. 2. The growth rate of modulation G_6 versus frequency Ω for the sixth-order NLS Eq. (2) with $\omega = 0, 1, 2,$ respectively.

contains two different regions, MI and MS. The expression $\Omega^2 - 4A^2$ in G_6 indicates that a low-perturbed frequency MI band ($|\Omega| < 2A$) exists in the frequency plane (ω, Ω). Setting $A = 1$ and $\delta_6 = 0.05,$ there are two MS quasi-elliptic rings in frequency plane (ω, Ω), which is demonstrated by Fig. 1(e). When selecting suitable parameters so that the elliptical semi-major axis is greater than 2, then there exist four curves in the MI band. With selecting of $\delta_6 = 0,$ Eq. (2) can be transformed into classical NLS equation and the corresponding MI gain G_6 is reduced to $\frac{1}{2}Im\left(|\Omega|\sqrt{(\Omega^2 - 4A^2)}\right)$. Fig. 1(a) displays the MI gain distribution features of classical NLS equation, which has obviously neither MS curve nor MS quasi-elliptic ring in the MI band.

Table 1
Relation between three parameters.

The Nonlinear Schrödingner equation with higher-order terms									
The order of dispersion term	2	3	4	5	6	7	8	...	n
The highest power of ω in g_i function	0	1	2	3	4	5	6	...	n-2
The number of the MS curves in MI band	0	1	2	3	4	5	6	...	n-2

From Eq. (6), we can see that the gain function G_6 depends on free parameters A, δ_6 and ω. It is shown in Fig. 2 for different values of ω and fixed $A = 1$, $\delta_6 = 0.05$. It is clear that these gain curves are symmetrical about $\Omega = 0$, as Fig. 2 shows. For $\omega = 0$, the growth rate can reach zero at $\Omega = 0, \pm 2$. The gain curve has two local maxima at $\Omega = \pm 1.0736$. For $\omega = 1$, the green line curve can reach zero at the same point as the case of $\omega = 0$, and the maximum gain occurs at $\Omega = \pm 1.0707$. In addition to the three points above, for $\omega = 2$, there are two other points, $\Omega = \pm 1.2457$, where the gain G_6 is equal to 0. For $\omega = 2$, the blue dot-dashed curve has four local maxima at four points, $\Omega = \pm 0.6895$ and $\Omega = \pm 1.8219$. The shape of the gain curve in last case is obviously different from the first two cases.

By discussing the influence of different higher-order terms on the MI gain distribution, we have the expression $G_i(i = 2, 3, \cdots)$ including a factor $\frac{1}{2} Im\left(|\Omega|\sqrt{(\Omega^2 - 4A^2)}\right)$ and a polynomial g_i. A determines the range of the MI gain, and g_i determines the MS curve distribution. In the present paper, we consider MI of the standard NLS equation just with only one higher-order term, and then compare it with the standard NLS equation. It is not difficult to find that the higher-order term determines the power of polynomial g_i, which has a great influence on the distribution of MI, so the higher-order term plays a crucial role in the MI feature. From the standard NLS equation to eighth-order dispersion NLS equation, the number of the MS curves is 0,1,2,3,4,5,6, respectively; and the highest power of g_i is also 0,1,2,3,4,5,6, respectively. Finally, a relationship between the order of the dispersion term, the highest degree of the polynomial g_i with respect to ω, and the number of MS curves is shown in Table 1.

3. Generalized Darboux Transformation for the sixth-order NLS equation

In this section, we will construct a generalized DT to obtain the rational solution for the sixth-order NLS Eq. (2). The linear spectral problem of Eq. (2) with $j = 6$ in [30] can be expressed as follows

$$\Psi_t = i(\lambda\sigma_1 + Q)\Psi, \quad \Psi_z = \sum_{c=0}^{6} i\lambda^c V_c \Psi, \tag{9}$$

where

$$\sigma_1 = \begin{pmatrix} 1 & 0 \\ 0 & -1 \end{pmatrix}, \quad Q = \begin{pmatrix} 0 & q^* \\ q & 0 \end{pmatrix}, \quad V_c = \begin{pmatrix} A_c & B_c^* \\ B_c & -A_c \end{pmatrix},$$

with

$$\begin{aligned}
A_0 &= -\frac{1}{2}|q|^2 - 10\delta_6|q|^6 - 5\delta_6[q^2(q_t^*)^2 + (q^*)^2 q_t^2] - 10\delta_6|q|^2(qq_{tt}^* + q^*q_{tt}) - \delta_6|q_{tt}|^2 + \delta_6(q_tq_{ttt}^* + q_t^*q_{ttt} - q^*q_{tttt} - qq_{tttt}^*),\\
A_1 &= 12i\delta_6|q|^2(q_tq^* - q_t^*q) + 2i\delta_6(q_tq_{tt}^* - q_t^*q_{tt} + q^*q_{ttt} - q_{ttt}^*q), \quad A_2 = 1 + 12\delta_6|q|^4 - 4\delta_6|q_t|^2 + 4\delta_6(q_{tt}^*q + q_{tt}q^*),\\
A_3 &= 8i\delta_6(qq_t^* - q^*q_t), \quad A_4 = -16\delta_6|q|^2, \quad A_5 = 0, \quad A_6 = 32\delta_6, \quad B_2 = -24i\delta_6|q|^2q_t - 4i\delta_6q_{ttt}, \quad B_4 = 16i\delta_6q_t,\\
B_0 &= \frac{i}{2}q_t + i\delta_6q_{ttttt} + 10i\delta_6(qq_t^*q_{tt} + qq_{tt}^*q_t + |q|^2q_{ttt} + 3|q|^4q_t + q_t|q_t|^2 + 2q^*q_tq_{tt}), \quad B_3 = -16\delta_6|q|^2q - 8\delta_6q_{tt},\\
B_1 &= q + 12\delta_6q^*q_t^2 + 16\delta_6|q|^2q_{tt} + 4\delta_6q^2q_{tt}^* + 2\delta_6q_{tttt} + 12\delta|q|^4q + 8\delta_6q|q_t|^2, \quad B_5 = 32\delta_6q, \quad B_6 = 0.
\end{aligned}$$

Here $\Psi = (\psi, \phi)^\dagger$ is the vector eigenfunction of the linear spectral problem (9) with spectral parameter λ, ψ and ϕ denote complex functions with z and t, † means matrix transpose and * denotes the complex conjugation. It is clearly that $U_z - V_t + UV - VU = 0$, which is the compatibility condition of (9) and can directly give rise to Eq. (2).

Suppose that $\Psi_1 = (\psi_1, \phi_1)\dagger$ is a fundamental vector solution of the linear spectral problem (9) with $q = q[0]$ and $\lambda = \lambda_1$. Then the basic DT for Eq. (2) has the form

$$\begin{aligned}
&\Psi[1] = T[1]\Psi, \quad T[1] = \lambda I - H[0]\Lambda_1 H[0]^{-1},\\
&q[1] = q[0] + 2(\lambda_1^* - \lambda_1)\frac{\psi_1[0]^*\phi_1[0]}{(|\psi_1[0]|^2 + |\phi_1[0]|^2)},
\end{aligned} \tag{10}$$

where $\phi_1[0] = \phi_1$, $\psi_1[0] = \psi_1$, and

$$I = \begin{pmatrix} 1 & 0 \\ 0 & 1 \end{pmatrix}, \quad H[0] = \begin{pmatrix} \psi_1[0] & -\phi_1[0]^* \\ \phi_1[0] & \psi_1[0]^* \end{pmatrix}, \quad \Lambda_1 = \begin{pmatrix} \lambda_1 & 0 \\ 0 & \lambda_1^* \end{pmatrix}.$$

In the general case, assume similarly that $\Psi_l = (\psi_l, \phi_l)^\dagger$, $1 \le l \le N$ represent N elementary solutions to (9) with $q = q[0]$ and $\lambda = \lambda_l$. Then N-fold basic DT for Eq. (2) is thereby inferred that

$$\begin{aligned} &\Psi[N] = T[N]T[N-1]T[N-2]\cdots T[1]\Psi, \quad T[l] = \lambda I - H[l]\Lambda_l H[l]^{-1}, \\ &q[N] = q[N-1] + 2(\lambda_N^* - \lambda_N)\frac{\psi_N[N-1]^*\phi_N[N-1]}{(|\psi_N[N-1]|^2 + |\phi_N[N-1]|^2)}, \end{aligned} \tag{11}$$

where $\Psi_l[l-1] = (\psi_l[l-1], \phi_l[l-1])^\dagger$, and

$$\begin{aligned} &\Psi_l[l-1] = T_l[l-1]T_l[l-2]T_l[l-3]\cdots T_l[1]\Psi_l, \quad T_l[k] = T[k]|_{\lambda=\lambda_l}, \\ &H[l-1] = \begin{pmatrix} \psi_l[l-1] & -\phi_l[l-1]^* \\ \phi_l[l-1] & \psi_l[l-1]^* \end{pmatrix}, \quad \Lambda_l = \begin{pmatrix} \lambda_l & 0 \\ 0 & \lambda_l^* \end{pmatrix}, \quad 1 \le l \le N, 1 \le k \le l-1. \end{aligned}$$

Considering an elementary solution cannot be iterated many times by the above method, it is necessary to construct the generalized DT [36] to overtake this difficulty. Therefore, suppose that $\Psi_1 = \Psi_1(\lambda_1 + \epsilon)$ is a special solution of (9) with $q[0]$ at $\lambda = \lambda_1 + \epsilon$. Applying the Taylor expansion on Ψ_1 at $\epsilon = 0$, it yields

$$\Psi_1 = \Psi_1^{[0]} + \Psi_1^{[1]}\epsilon + \Psi_1^{[2]}\epsilon^2 + \Psi_1^{[3]}\epsilon^3 + \cdots + \Psi_1^{[N]}\epsilon^N + \cdots, \tag{12}$$

with ϵ a small parameter and $\Psi_1^{[k]} = \frac{1}{k!}\frac{\partial^k}{\partial\lambda^k}\Psi_1(\lambda)|_{\lambda=\lambda_1}$. It is obvious that $\Psi_1^{[0]}$ is the solution of (9) with $q = q[0]$ at $\lambda = \lambda_1$.

3.1. The 1-fold generalized DT

According to the basic DT (10), we can easily derive the 1-fold generalized DT formulas, that is

$$\begin{aligned} &\Psi[1] = T[1]\Psi, \quad T[1] = \lambda I - H[0]\Lambda_1 H[0]^{-1}, \\ &q[1] = q[0] + 2(\lambda_1^* - \lambda_1)\frac{\psi_1[0]^*\phi_1[0]}{(|\psi_1[0]|^2 + |\phi_1[0]|^2)}, \end{aligned} \tag{13}$$

with $\phi_1[0] = \phi_1^{[0]}$, $\psi_1[0] = \psi_1^{[0]}$, and

$$H[0] = \begin{pmatrix} \psi_1[0] & -\phi_1[0]^* \\ \phi_1[0] & \psi_1[0]^* \end{pmatrix}, \quad \Lambda_1 = \begin{pmatrix} \lambda_1 & 0 \\ 0 & \lambda_1^* \end{pmatrix}.$$

3.2. The 2-fold generalized DT

Apparently, $T[1]\Psi_1$ is the new solution of the Lax pair (9) with $q[1]$ at $\lambda = \lambda_1 + \epsilon$ and $T_1[1]\Psi_1^{[0]} = 0$. With the limit

$$\begin{aligned} \lim_{\epsilon\to 0}\frac{T[1]|_{\lambda=\lambda_1+\epsilon}\Psi_1}{\epsilon} &= \lim_{\epsilon\to 0}\frac{(\epsilon + T_1[1])\Psi_1}{\epsilon} \\ &= \Psi_1^{[0]} + T_1[1]\Psi_1^{[1]} \equiv \Psi_1[1], \end{aligned}$$

it gives a nonzero solution of (9) with $q[1]$ at $\lambda = \lambda_1$. Hence, 2-fold generalized DT can be constructed

$$\begin{aligned} &\Psi[2] = T[2]T[1]\Psi, \quad T[2] = \lambda I - H[1]\Lambda_2 H[1]^{-1}, \\ &q[2] = q[1] + 2(\lambda_1^* - \lambda_1)\frac{\psi_1[1]^*\phi_1[1]}{(|\psi_1[1]|^2 + |\phi_1[1]|^2)}, \end{aligned} \tag{14}$$

with $\Psi_1[1] = (\psi_1[1], \phi_1[1])^\dagger$, and

$$H[1] = \begin{pmatrix} \psi_1[1] & -\phi_1[1]^* \\ \phi_1[1] & \psi_1[1]^* \end{pmatrix}, \quad \Lambda_2 = \begin{pmatrix} \lambda_1 & 0 \\ 0 & \lambda_1^* \end{pmatrix}.$$

3.3. The 3-fold generalized DT

Continuing the similar process above, we give 3-fold generalized DT. Under the following conditions

$$T_1[1]\Psi_1^{[0]} = 0, \quad T_1[2](\Psi_1^{[0]} + T_1[1]\Psi_1^{[1]}) = 0,$$

and applying the limit

$$\begin{aligned} \lim_{\epsilon\to 0}\frac{[T[2]T[1]]|_{\lambda=\lambda_1+\epsilon}\Psi_1}{\epsilon^2} &= \lim_{\epsilon\to 0}\frac{(T_1[2]+\epsilon)(T_1[1]+\epsilon)\Psi_1}{\epsilon^2} \\ &= \Psi_1^{[0]} + (T_1[1] + T_1[2])\Psi_1^{[1]} + T_1[2]T_1[1]\Psi_1^{[2]} \\ &\equiv \Psi_1[2], \end{aligned}$$

a nontrivial solution can be obtained for the Lax pair (9) with $q[2]$ at $\lambda = \lambda_1$. Then the 3-fold generalized DT is naturally deduced as follows

$$\begin{aligned}
&\Psi[3] = T[3]T[2]T[1]\Psi, \quad T[3] = \lambda I - H[2]\Lambda_3 H[2]^{-1},\\
&q[3] = q[2] + 2(\lambda_1^* - \lambda_1)\frac{\psi_1[2]^*\phi_1[2]}{(|\psi_1[2]|^2 + |\phi_1[2]|^2)},
\end{aligned} \tag{15}$$

where $\Psi_1[2] = (\psi_1[2], \phi_1[2])^\dagger$, and

$$H[2] = \begin{pmatrix} \psi_1[2] & -\phi_1[2]^* \\ \phi_1[2] & \psi_1[2]^* \end{pmatrix}, \quad \Lambda_3 = \begin{pmatrix} \lambda_1 & 0 \\ 0 & \lambda_1^* \end{pmatrix}.$$

3.4. The N-fold generalized DT

Iterating N times of the above process, it naturally gives rise to the expression of N-fold generalized DT, which reads

$$\begin{aligned}
&\Psi_1[N-1] = \Psi_1^{[0]} + \sum_{l=1}^{N-1} T_1[l]\Psi_1^{[1]} + \sum_{k=1}^{l-1}\sum_{l=1}^{N-1} T_1[l]T_1[k]\Psi_1^{[2]} + \cdots + T_1[N-1]T_1[N-2]\cdots T_1[1]\Psi_1^{[N-1]},\\
&\Psi[N] = T[N]T[N-1]T[N-2]\cdots T[1]\Psi, \quad T[N] = \lambda I - H[N-1]\Lambda_N H[N-1]^{-1},\\
&q[N] = q[N-1] + 2(\lambda_1^* - \lambda_1)\frac{\psi_1[N-1]^*\phi_1[N-1]}{(|\psi_1[N-1]|^2 + |\phi_1[N-1]|^2)},
\end{aligned} \tag{16}$$

where $\Psi_1[N-1] = (\psi_1[N-1], \phi_1[N-1])^\dagger$, and

$$H[l-1] = \begin{pmatrix} \psi_1[l-1] & -\phi_1[l-1]^* \\ \phi_1[l-1] & \psi_1[l-1]^* \end{pmatrix}, \quad \Lambda_l = \begin{pmatrix} \lambda_1 & 0 \\ 0 & \lambda_1^* \end{pmatrix}, 1 \le l \le N.$$

Combining the above formulas 13–(16), it follows a compact formula for N-order rational solution of (2) that

$$q[N] = q[0] + 2(\lambda_1^* - \lambda_1)\sum_{j=0}^{N-1}\frac{\psi_1[j]^*\phi_1[j]}{(|\psi_1[j]|^2 + |\phi_1[j]|^2)}. \tag{17}$$

It is necessary to mention that the seed solution $q[0]$ and its corresponding vector solution $(\psi_1[j], \phi_1[j])^\dagger$ of the Lax pair (9) with the spectral parameter $\lambda = \lambda_1$ are specified data that must be chosen to get the explicit solution (17). In the following section, we will utilize the above formula to derive rogue wave solutions and analyze their dynamic behavior.

4. Rogue wave solutions

Having established the result of generalized DT, attention is now given to constructing higher-order rogue wave solutions for (2). For this purpose, we choose the following seed solution

$$q[0] = e^{i\theta}, \quad \theta = at + (-a^6\delta_6 + 30a^4\delta_6 - 90a^2\delta_6 - \frac{1}{2}a^2 + 20\delta_6 + 1)z, \quad a \in \mathbb{R}. \tag{18}$$

The problem that a seed solution cannot be iterated by basic DT, can be solved by constructing its generalized DT. By substituting Eq. (18) into Eq. (9), the corresponding fundamental vector solution can be obtained, that is

$$\Psi_1 = \begin{pmatrix} i(C_1e^M - C_2e^{-M})e^{-\frac{i}{2}\theta} \\ (C_2e^M - C_1e^{-M})e^{\frac{i}{2}\theta} \end{pmatrix}, \tag{19}$$

with

$$\begin{aligned}
C_1 &= \frac{(a+2\lambda+\sqrt{(a+2\lambda)^2+4})^{\frac{1}{2}}}{\sqrt{(a+2\lambda)^2+4}}, \quad C_2 = \frac{(a+2\lambda+\sqrt{(a+2\lambda)^2+4})^{\frac{1}{2}}}{\sqrt{(a+2\lambda)^2+4}},\\
M &= \frac{1}{4}\sqrt{(a+2\lambda)^2+4}\Big\{[i(-2a^5 + 4a^4\lambda - 8a^3\lambda^2 + 16a^2\lambda^3 - 32a\lambda^4 + 64\lambda^5 + 40a^3 - 48a^2\lambda\\
&\quad + 48a\lambda^2 - 32\lambda^3 - 60a + 24\lambda)\delta_6 + i(-a+2\lambda)]z + 2it + \sum_{k=1}^{N} s_k\xi^{2k}\Big\}, \quad s_k = m_k + in_k, (m_k, n_k \in \mathbb{R}),
\end{aligned}$$

where ξ is a small real parameter [36]. Setting $\lambda = -\frac{1}{2}a + i + \xi^2$ and expanding Ψ_1 at $\xi = 0$, it has

$$\Psi_1(\xi) = \Psi_1^{[0]} + \Psi_1^{[1]}\xi^2 + \Psi_1^{[2]}\xi^4 + \cdots. \tag{20}$$

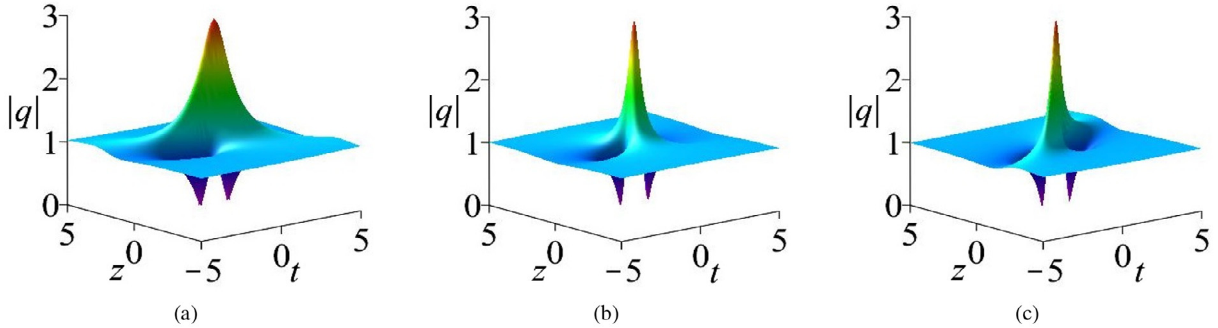

Fig. 3. Plots of first-order rogue wave with $a = -0.5, 0, 0.5$, from left to right, respectively and $\delta_6 = 0.01$.

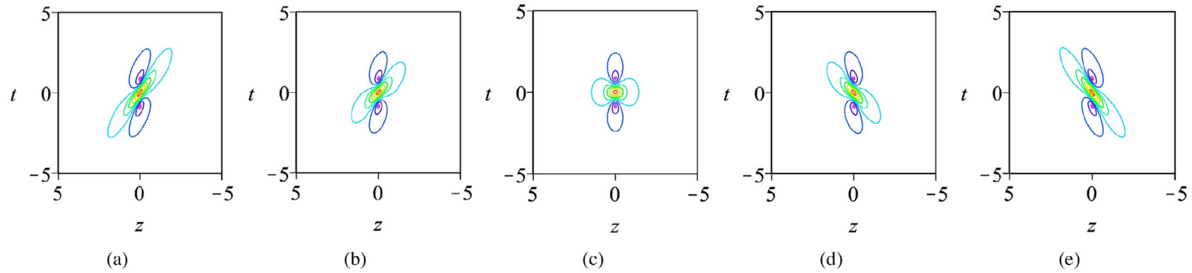

Fig. 4. Contour graphics of the first-order rogue wave with $a = -0.5, -0.3, 0, 0.3, 0.5$, from left to right, respectively and $\delta_6 = 0.01$.

Here, vector function $\Psi_1^{[0]}$ has the following explicit expression

$$\psi_1^{[0]} = \frac{1+i}{2}\eta_1^{[0]}e^{-\frac{i}{2}\theta}, \quad \phi_1^{[0]} = -\frac{1+i}{2}\eta_2^{[0]}e^{\frac{i}{2}\theta}, \tag{21}$$

where

$$\begin{aligned}\eta_1^{[0]} &= 12(a^5 - 5ia^4 - 20a^3 + 30ia^2)\delta_6 + 2(180\delta_6 + 1)a - 2i(60\delta_6 + 1),\\ \eta_2^{[0]} &= 12(ia^5 + 5a^4 - 20ia^3 - 30a^2)\delta_6 + 2i(180\delta_6 + 1)a + 2(60\delta_6 + 1).\end{aligned}$$

Clearly, $\Psi_1^{[0]} = (\psi_1^{[0]}, \phi_1^{[0]})^\dagger$ satisfies the system (9) with spectral parameter $\lambda_1 = -\frac{a}{2} + i$. Therefore, utilizing the formula (17) with $N = 1$, it suffices to obtain first-order rogue wave solution of (2),

$$q[1] = \left(1 + \frac{D_1 + iE_1}{F_1}\right)e^{i\theta}, \tag{22}$$

where

$$\begin{aligned}F_1 &= 144(a^{10} - 15a^8 + 160a^6 - 200a^4 + 300a^2 + 100)z^2\delta_6^2 + 48(a^6 - 15a^4 + 10)z^2\delta_6\\ &\quad -48(a^4 - 20a^2 + 30)azt\delta_6 + 4(a^2 + 1)z^2 - 8azt + 4t^2 + 1,\\ D_1 &= -288(a^{10} - 15a^8 + 160a^6 - 200a^4 + 300a^2 + 100)z^2\delta_6^2 - 96(a^6 - 15a^4 + 10)z^2\delta_6\\ &\quad +96(a^4 - 20a^2 + 30)azt\delta_6 - 8(a^2 + 1)z^2 + 16azt - 8t^2 + 2,\\ E_1 &= 240(a^4 - 6a^2 + 2)z\delta_6 + 8z.\end{aligned}$$

Obviously, there are two arbitrary parameters a and δ_6 in the expression $q[1]$, the latter is the sixth-order dispersion coefficient. We fix δ_6 to analyze the effect of frequency a on the dynamic behavior of the rogue waves. Taking the case of $a = 0$ as a criterion, when $a < 0$, the crest of rogue wave occurs counterclockwise deflection; while $a > 0$, the crest occurs clockwise deflection, and the width of the crest also changes. In addition, when $|a|$ increases, the deflection angle of crest of rogue wave increases, and so does its width. Figs. 3 and 4 illustrate the above dynamic characteristics. Now, fixing a to be any particular constant and taking limit on $q[1]$ at $\delta_6 \to \infty$, that is

$$\lim_{|\delta_6|\to\infty} |q[1]| \equiv 1. \tag{23}$$

As the absolute value of δ_6 increases, the modulus of $q[1]$ gradually reverts to a constant background plane. In other word, the rogue wave gradually disappears and the energy gradually decreases. Without loss of generality, fixing $a = 0$, Fig. 5

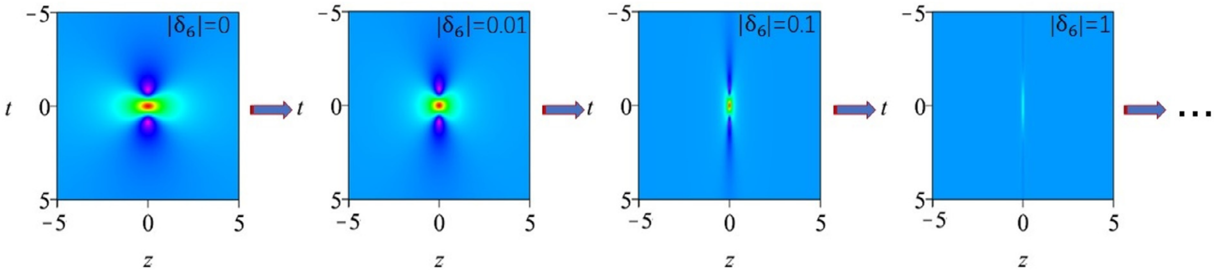

Fig. 5. The evolution process of the rogue wave structure with the change of δ_6 for $a = 0$.

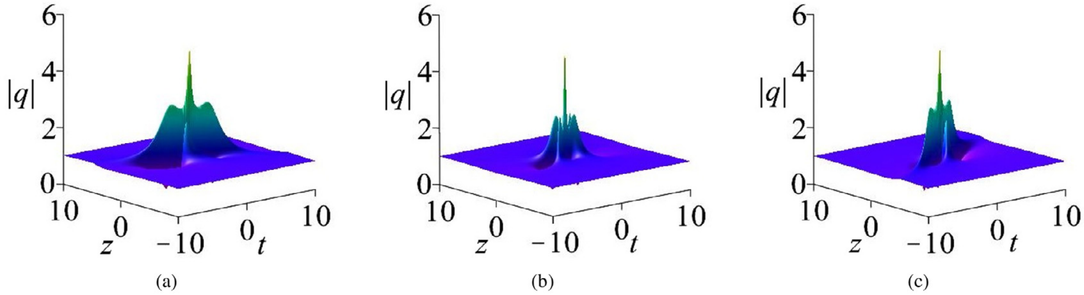

Fig. 6. Plots of second-order rogue wave by choosing $m_1 = n_1 = 0$ and $a = -0.5, 0, 0.5$, from left to right, respectively.

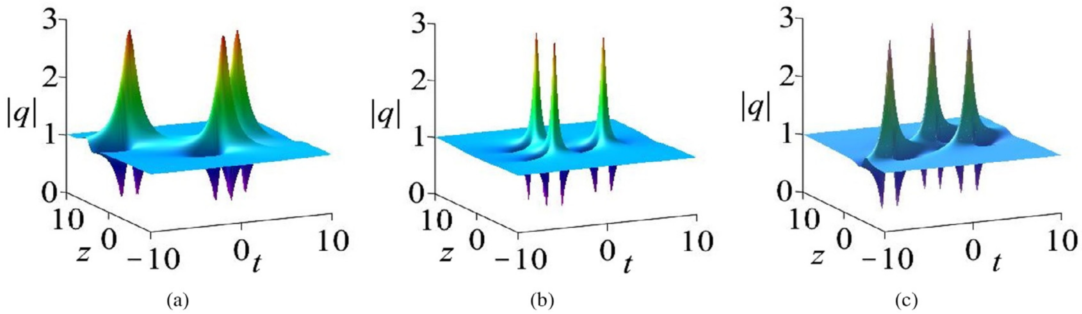

Fig. 7. 3D graphics of the second-order rogue wave by choosing $\delta_6 = 0.01$, $m_1 = 100$, $n_1 = 0$ and $a = -0.5$, 0, 0.5, from left to right, respectively.

shows the evolution process of the first-order rogue wave structure with the parameter δ_6. When $\delta_6 = 0$, Eq. (1) degenerates into the standard NLS equation, and it follows that the amplitude of $|q[1]|$ is equal to 3.

Similar to the computational process of Section 3.2, taking limit

$$\begin{aligned}\lim_{\xi\to 0}\frac{T[1]|_{\xi=-\frac{1}{2}a+i+\xi^2}\Psi_1}{\xi^2} &= \lim_{\xi\to 0}\frac{(\xi^2+T_1[1])\Psi_1}{\xi^2}\\ &= \Psi_1^{[0]}+T_1[1]\Psi_1^{[1]}\\ &\equiv \Psi_1[1],\end{aligned}\tag{24}$$

and using the obtained formula (17) with $N = 2$, it is not difficult to deduce the concrete expression of the second-order rogue wave solution. Since the expression of this solution is too cumbersome, we only show its dynamic behavior, which are illustrated by Figs. 6 and 7. They present two kinds of rogue wave structures, and have different dynamic behavior. The corresponding contour map of Fig. 7 is demonstrated in Fig. 8.

Substituting $m_1 = 0, n_1 = 0$ into Eq. (17), the second-order fundamental rogue wave solution can be derived, and there exists a maximum value 5 at point (0,0) in the (t, z) plane, see Fig. 6. However, when only changing a parameter $m_1 = 100$, the fundamental structure disappears, there appears a triplet structure containing three first-order rogue waves. Similarly, the deflation properties in first-order rogue wave also exist in the above two kinds of second-order rogue wave structures. The evolution process of this corresponding rogue wave structure is demonstrated in Fig. 8 with different values of amplitude a.

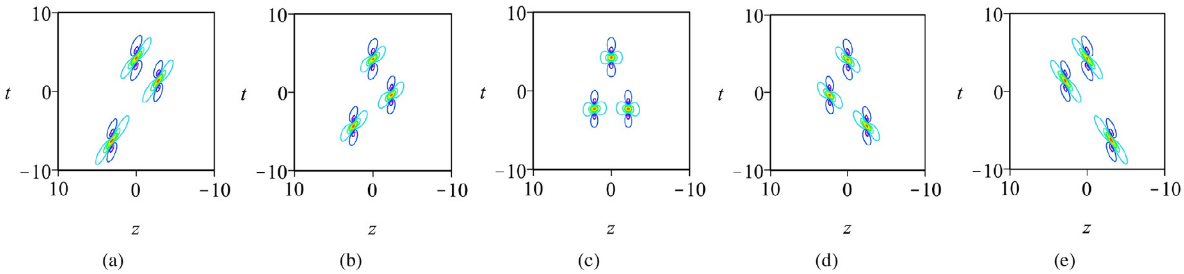

Fig. 8. The corresponding contour graphics for the second-order rogue wave obtained in Fig. 7 with parameters: $\delta_6 = 0.01$, $m_1 = 100$, $n_1 = 0$ and $a = -0.5$, -0.3, 0,0.3, 0.5, from left to right, respectively.

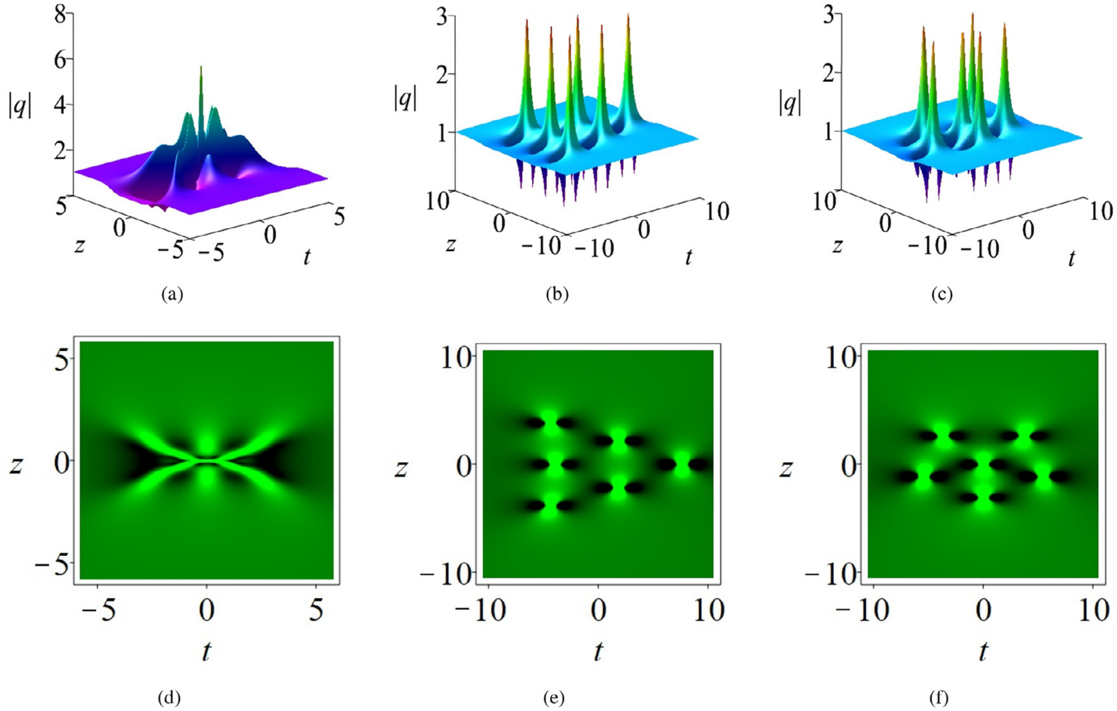

Fig. 9. Three kinds of third-order rogue wave structures for Eq. (2). Left columns: fundamental type structure at $a = 0, \delta_6 = 0.01, m_i = n_i = 0 \ (i = 1, 2)$; middle columns: triangular structure at $m_1 = 100$, the rest of the parameters are same to left columns; right columns: circular structure at $m_2 = 1000$, the rest of the parameters are same to left columns.

Applying formula (17) with $N = 3$, it then yields the third-order rogue wave solution. Here, we just show three types of third-order rogue wave solutions, fundamental pattern, triangular pattern and circular pattern rogue waves, respectively, see Fig. 9. The first row is the three-dimensional graphs, and the second row is the corresponding density maps. The amplitude of the third-order fundamental rogue wave reaches maximum value 7 at point (0,0) in the (t, z) plane. Obviously, these rogue waves are symmetrical, which can be seen from Figs. 9(d-f). They also possess the above deflection characteristics. In short, when $N > 1$, the higher-order rogue waves with different structures can be obtained by choosing appropriate values of the parameters m_k and n_k.

5. Spectral analysis of rogue waves

Our attention is now turned to spectral analysis of rogue wave solution for Eq. (22) in this section. In [54], it appears that the specific triangular spectrum for a Peregrine rogue wave could be applied to early warning of rogue waves by spectral measurements. The spectral analysis is referred to as a useful method in predicting and exciting rogue wave solutions in the nonlinear fiber [55,56]. In order to calculate the spectrum of first-order rogue wave solution more conveniently, we take $\delta_6 = \frac{1}{12}$ in Eq. (22). It then follows that

$$q[1] = \left(\frac{4(1 + iK_1)}{K_2} - 1 \right) \exp(i\theta_0), \tag{25}$$

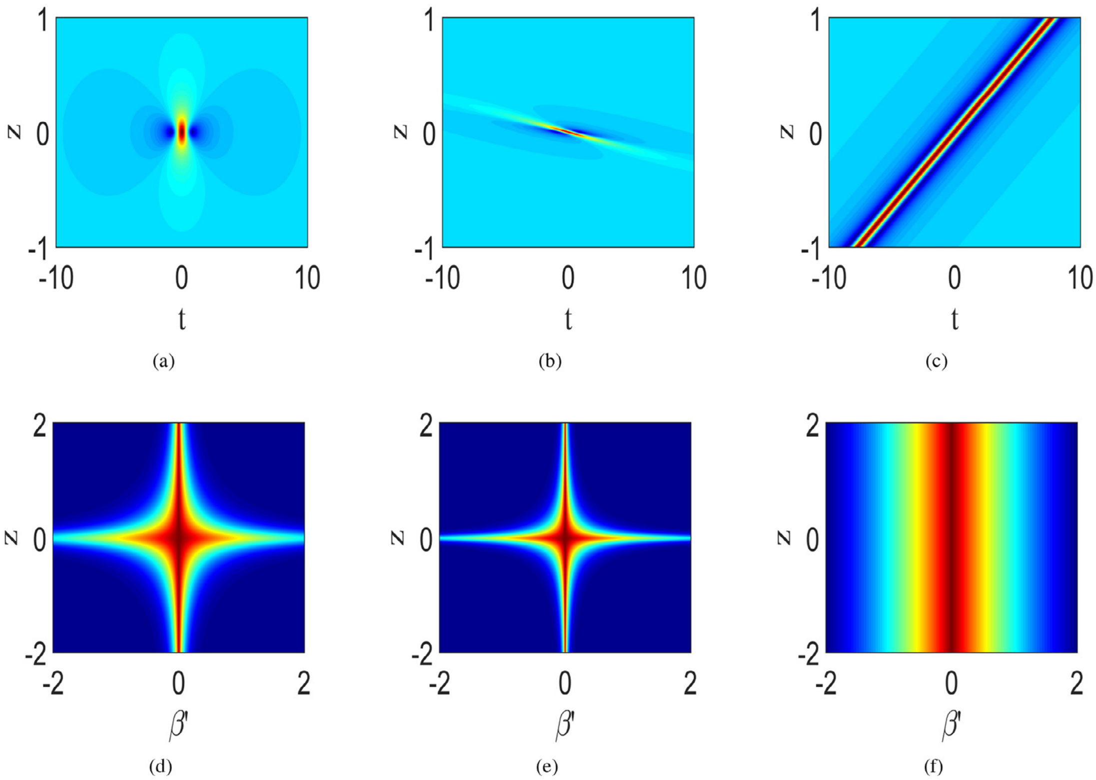

Fig. 10. The first row displays density figures of two first-order rogue waves and a W-shaped soliton solution in Eq. (25) with $a = 0$, 2, and $\frac{1}{5}\sqrt{75 - \sqrt{165}}$, from left to right, respectively. The bottom row displays the spectrum evolution of $|F(\beta, z)|$ in Eq. (27).

where

$$K_1 = (5a^4 - 30a^2 + 12)z, \qquad \theta_0 = at + \left(\frac{5}{2}a^4 - \frac{97}{12}a^2 + \frac{8}{3}\right)z,$$
$$K_2 = (a^{10} - 15a^8 + 160a^6 - 260a^4 + 304a^2 + 144)z^2 - 4(a^4 - 20a^2 + 32)azt + 4t^2 + 1.$$

Now we perform spectral analysis approach on the above derived first-order rogue wave solution by the Fourier transformation as follows

$$F(\beta, z) = \frac{1}{\sqrt{2\pi}} \int_{-\infty}^{+\infty} q[1](z, t) \exp(i\beta t) dt. \tag{26}$$

From the solution (25), it is inferred that the rogue wave solution contains two parts, a plane wave and a variable signal part. It is clear that the plane wave background becomes infinity and the integral is a δ function, so we omit the spectrum of plane wave background. The corresponding modulus of the rogue wave signal is given by

$$|F(\beta, z)| = \sqrt{2\pi} \exp\left(-\frac{|\beta'|}{2}\sqrt{1 + (5a^4 - 30a^2 + 12)^2 z^2}\right), \tag{27}$$

where $\beta' = \beta + a$.

Firstly, from the perspective of the bottom row in Fig. 10, it is clear that the spectrum of the solution (25) with different a has strong symmetry property. And then combined with the expression (27), when $a \neq \pm\frac{1}{5}\sqrt{75 \pm 5\sqrt{165}}$, Fig. 10(d) and (e) have specific triangular spectrum of a Peregrine rogue wave. Furthermore, one can easily find that the triangular widening appears at $a = 0$, when compared to the case at $a = 2$. The corresponding density diagrams are displayed in Fig. 10(a) and (b). However, when $a = \pm\frac{1}{5}\sqrt{75 \pm 5\sqrt{165}}$, the spectrum of the solution (25) possess a band structure, see Fig. 10(f), and the rogue wave solution is now reduced to a stable W-shaped soliton solution in Fig. 10(c). Similarly, N-order rogue waves can be reduced to N-order W-shaped solitons. This result in turn implies that MI analysis is consistent with spectral analysis for the sixth-order Eq. (2) with $\delta_6 = \frac{1}{12}$. From the perspective of MI gain function (6), it can be adduced that

$$g_6 = \frac{1}{6}(30A^4 - 10\Omega^2 A^2 - 90a^2 A^2 + \Omega^4 + 15a^2\Omega^2 + 15a^4 + 6), \tag{28}$$

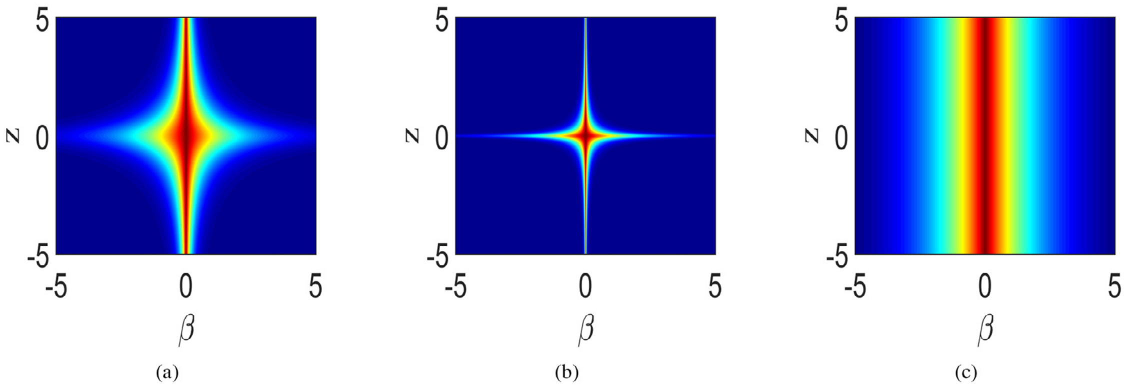

Fig. 11. Spectrum evolution of $|F(\beta, z)|$ in Eq. (31) with $\delta_6 = 0$, 0.1 and $-\frac{1}{60}$, from left to right, respectively.

where A is the amplitude, Ω is the perturbed frequency and a is the frequency of background. By setting $A = 1, \Omega = 0$ and $g_6 = 0$, it follows

$$g_6 = \frac{1}{2}(5a^4 - 30a^2 + 12) = 0, \tag{29}$$

then there occurs a transition of two sates here, which happens between the rogue wave and the W-shaped soliton in the region of zero-frequency MS.

In order to demonstrate the impact of the parameter δ_6, we will give the spectral analysis of the rogue wave solution by selecting $a = 0$ in Eq. (22) for convenience. It thus transpires that

$$q[1] = \left(\frac{4(1 + 2i(1 + 60\delta_6)z)}{4t^2 + 4(1 + 60\delta_6)^2 z^2 + 1} - 1\right)\exp(i(1 + 20\delta_6)z), \tag{30}$$

and

$$|F(\beta, z)| = \sqrt{2\pi}\exp\left(-\frac{|\beta|}{2}\sqrt{1 + 4(1 + 60\delta_6)^2 z^2}\right). \tag{31}$$

Similarly, when $\delta_6 \neq -\frac{1}{60}$, the spectrum structure of the solution (30) also possesses specific triangular spectrum of a Peregrine rogue wave. In addition, their spectrums have the same features with different parameters as Eq. (25). By comparing Fig. 10(d-f) with Fig. 11, it is obvious that the small change of δ_6 will lead to a big change in the corresponding triangular spectrum structure. When $\delta_6 = -\frac{1}{60}$, the solution (30) degenerates into a W-shaped soliton, and the corresponding spectrum appears in a banded form, which is presented in Fig. 11(c).

6. Summary and discussions

In conclusion, Modulation instability, rogue wave and spectral analysis are studied for the nonlinear Schrödinger equation with higher-order terms. MI of the continuous wave background has been investigated for the NLS equation with different higher-order dispersion terms. The MI distribution characteristics for the sixth-order to the eighth-order NLS equations are studied in detail. There are two arbitrary parameters, namely, higher-order dispersion term $\delta_i, i = 3, 4, \ldots$ and amplitude A. These parameters control the MS distribution of the NLS with different higher-order dispersion terms in the MI band. By adjusting the parameters, the MS quasi-elliptic and MS elliptic ring can be completely contained within the MI band or intersected at the MI boundary, the latter case yields two curves in the MI band. g_i is a polynomial with ω, and its highest power of ω is closely related to the number of MS curves in the MI band. It is adduced that the higher-order dispersion terms indeed affect the distribution of the MS regime, n-order dispersion term corresponds to $n - 2$ modulation stability curves in the MI band. Here, we do not consider the case of NLS equation with multiple dispersion terms, only considering the case with a higher-order dispersion term. It is inferred that the distribution of MS curve in the MI band is not affected. Therefore, when multiple different dispersion terms exist simultaneously, the higher-order dispersion term plays the main role in the distribution of MS curve in the MI band.

Then we construct a generalized DT for the sixth-order NLS equation and derive a compact algebraic expression of N-order rogue waves. The specific expression of first-order rogue wave is derived. Since expressions of higher-order rogue waves are too cumbersome, we only demonstrate the dynamic behavior through pictures. There are two arbitrary parameters a and δ_6 existing in the rogue wave solutions, the sign of the former determines the direction of deflection and the magnitude of the absolute value affects the angle of deflection and the width of rogue wave solution. While the latter can cause the change of the width and amplitude of rogue wave. For the first- to third-order rogue waves, they all own the deflection properties mentioned above. For the third-order rogue wave solution, three kinds of structures, that is fundamental, triangular, and circular, are illustrated in Fig. 9, and their dynamic features are discussed in detail.

In addition, we analyze the spectral features of the first-order rogue wave and the conditions of the state transition between first-order rogue wave and W-shaped soliton. Via the spectral analysis approach on first-order rogue wave, it has been found that arbitrary parameters a and δ_6 have effects on the spectrum of the solution (25). Fixing $\delta_6 = \frac{1}{12}$ and $a \neq \pm\frac{1}{5}\sqrt{75 \pm 5\sqrt{165}}$, the solution has specific triangular spectrum for a Peregrine rogue wave and the value of a is related to the size of the triangular spectrum. While $a = \pm\frac{1}{5}\sqrt{75 \pm 5\sqrt{165}}$, the solution is reduced to a W-shaped soliton, which is not localized in temporal and spatial context and the spectrum is banded. Similarly, fixing a and δ_6 satisfying certain constraint, the spectrum of the solution (30) also presents the specific triangular spectrum or banded spectrum, which corresponding to the rogue wave solution or W-shaped soliton solution, respectively.

Finally, it is worthy to mention that we will further study the excitation conditions and numerical analysis of various nonlinear waves and their corresponding positions in the MI gain plane in the future. We hope that the above results will play a guiding role in the physics experiment.

Declaration of Competing Interest

The authors declare that they have no known competing financial interests or personal relationships that could have appeared to influence the work reported in this paper.

CRediT authorship contribution statement

Yunfei Yue: Writing - original draft, Writing - review & editing, Conceptualization, Formal analysis, Software. **Lili Huang:** Writing - review & editing, Conceptualization. **Yong Chen:** Writing - review & editing, Supervision, Project administration.

Acknowledgment

The project is supported by the National Natural Science Foundation of China (No. 11675054), Shanghai Collaborative Innovation Center of Trustworthy Software for Internet of Things (No. ZF1213), and Science and Technology Commission of Shanghai Municipality (No. 18dz2271000).

References

[1] Draper L. Freak wave. Mar Obs 1965;35:193–5.
[2] Kharif C, Pelinovsky E, Slyunyaev A. Quasi-linear wave focusing. In: Rogue waves in the ocean. Berlin: Springer; 2009. p. 63–89.
[3] Akhmediev N, Ankiewicz A, Taki M. Waves that appear from nowhere and disappear without a trace. Phys Lett A 2009;373:675–8.
[4] Benjamin TB, Feir JE. The disintegration of wave trains on deep water part 1. Theory J Fluid Mech 1967;27:417–30.
[5] Taniuti T, Washimi H. Self-trapping and instability of hydromagnetic waves along the magnetic field in a cold plasma. Phys Rev Lett 1968;21:209.
[6] Bespalov VI, Talanov VI. Filamentary structure of light beams in nonlinear liquids. Zh Eksp Teor Fiz Pis'ma Red 1966;3:471. English translation: JETP Lett. 3 (1966) 307
[7] Witham GB. Non-linear dispersive waves. Proc R Soc Lond A 1965;283:238–61.
[8] Zhao LC, Xin GG, Yang ZY. Rogue-wave pattern transition induced by relative frequency. Phys Rev E 2014;90:022918.
[9] Zhang JH, Wang L, Liu C. Superregular breathers, characteristics of nonlinear stage of modulation instability induced by higher-order effects. Proc R Soc A 2017;473:20160681.
[10] Wang X, Liu C, Wang L. Darboux transformation and rogue wave solutions for the variable-coefficients coupled hirota equations. J Math Anal Appl 2017;449:1534–52.
[11] Wang L, Zhang JH, Wang ZQ, Liu C, Li M, Qi FH, Guo R. Breather-to-soliton transitions, nonlinear wave interactions, and modulational instability in a higher-order generalized nonlinear schrödinger equation. Phys Rev E 2016;93:012214.
[12] Agrawal GP. Nonlinear fiber optics. New York: Academic; 2006.
[13] Stenflo L, Marklund M. Rogue waves in the atmosphere. J Plasma Phys 2010;76:293–5.
[14] Geist EL. Book review: Nonlinear ocean waves and the inverse scattering transform. Pure Appl Geophys 2011;168:1889–90.
[15] Peregrine DH. Water waves, nonlinear schrödinger equations and their solutions. J Aust Math Soc 1983;25:16–43.
[16] Akhmediev N, Ankiewicz A, Soto-Crespo JM. Rogue waves and rational solutions of the nonlinear schrödinger equation. Phys Rev E 2009;80:026601.
[17] Ankiewicz A, Clarkson PA, Akhmediev N. Rogue waves, rational solutions, the patterns of their zeros and integral relations. J Phys A: Math Theor 2010;43:122002.
[18] Ohta Y, Yang JK. General high-order rogue waves and their dynamics in the nonlinear schrödinger equation. Proc R Soc A 2012;468:1716–40.
[19] Proc R Soc A 2017;473:20170243.
[20] Gagnon L, Winternitz P. Symmetry classes of variable coefficient nonlinear schrödinger equations. J Phys A: Math Gen 1993;26:7061.
[21] Wang L, Zhang JH, Liu C, Li M, Qi FH. Breather transition dynamics, peregrine combs and walls, and modulation instability in a variable-coefficient nonlinear schrödinger equation with higher-order effects. Phys Rev E 2016;93:062217.
[22] Yang YQ, Wang X, Yan ZY. Optical temporal rogue waves in the generalized inhomogeneous nonlinear schrödinger equation with varying higher-order even and odd terms. Nonlinear Dyn 2015;81:833–42.
[23] Zhang GQ, Yan ZY. Three-component nonlinear schrödinger equations: modulational instability, nth-order vector rational and semi-rational rogue waves, and dynamics. Commun Nonlinear Sci Numer Simulat 2018;62:117–33.
[24] Xu T, Chen Y. Mixed interactions of localized waves in the three-component coupled derivative nonlinear schrödinger equations. Nonlinear Dyn 2018;92:2133–42.
[25] Zhang GQ, Yan ZY. The n-component nonlinear schrödinger equations: dark-bright mixed n-and high-order solitons and breathers, and dynamics. Proc R Soc A 2018;474:20170688.
[26] Yang B, Chen Y. Dynamics of high-order solitons in the nonlocal nonlinear schrödinger equations. Nonlinear Dyn 2018;94:489–502.
[27] Ankiewicz A, Wang Y, Wabnitz S, Akhmediev N. Extended nonlinear schrödinger equation with higher-order odd and even terms and its rogue wave solutions. Phys Rev E 2014;89:012907.
[28] Cai LY, Wang X, Wang L, Li M, Liu Y, Shi YY. Nonautonomous multi-peak solitons and modulation instability for a variable-coefficient nonlinear schrödinger equation with higher-order effects. Nonlinear Dyn 2017;90:2221–30.

[29] Bergé L. Wave collapse in physics: principles and applications to light and plasma waves. Phys Rep 1998;303:259–370.
[30] Kedziora DJ, Ankiewicz A, Chowdury A, Akhmediev N. Integrable equations of the infinite nonlinear schrödinger equation hierarchy with time variable coefficients. Chaos 2015;25:103114.
[31] Chowdury A, Ankiewicz A, Akhmediev N, Chang WK. Modulation instability in higher-order nonlinear schrödinger equations. Chaos 2018;28:123116.
[32] Ankiewicz A, Kedziora DJ, Chowdury A, Bandelow U, Akhmediev N. Infinite hierarchy of nonlinear schrödinger equations and their solutions. Phys Rev E 2016;93:012206.
[33] Hirota R. Exact envelope-soliton solutions of a nonlinear wave equation. J Math Phys 1973;14:805–9.
[34] Lakshmanan M, Porsezian K, Daniel M. Effect of discreteness on the continuum limit of the heisenberg spin chain. Phys Lett A 1988;133:483–8.
[35] Chowdury A, Kedziora DJ, Ankiewicz A, Akhmediev N. Soliton solutions of an integrable nonlinear schrödinger equation with quintic terms. Phys Rev E 2014;90:032922.
[36] Guo BL, Ling LM, Liu QP. Nonlinear schrödinger equation: generalized darboux transformation and rogue wave solutions. Phys Rev E 2012;85:026607.
[37] He JS, Zhang HR, Wang LH, Fokas AS. Generating mechanism for higher-order rogue waves. Phys Rev E 2013;87:052914.
[38] Wen XY, Yan ZY. Modulational instability and higher-order rogue waves with parameters modulation in a coupled integrable AB system via the generalized darboux transformation. Chaos 2015;25. 1231-15
[39] Wen XY, Yan ZY. Modulational instability and dynamics of multi-rogue wave solutions for the discrete ablowitz-ladik equation. J Math Phys 2018;59:073511.
[40] Wei J, Wang X, Geng XG. Periodic and rational solutions of the reduced maxwell-bloch equations. Commun Nonlinear Sci Numer Simulat 2018;59:1–14.
[41] Ling LM, Feng BF, Zhu ZN. Multi-soliton, multi-breather and higher-order rogue wave solutions to the complex short pulse equation. Physica D 2016;327:13–29.
[42] Su CQ, Gao YT, Xue L, Wang QM. Nonautonomous solitons, breathers and rogue waves for the gross-pitaevskii equation in the bose-einstein condensate. Commun Nonlinear Sci Numer Simulat 2016;36:457–67.
[43] Liu YB, Mihalache D, He JS. Families of rational solutions of the y-nonlocal davey-stewartson II equation. Nonlinear Dyn 2017;90:2445–55.
[44] Chen JC, Ma ZY, Hu YH. Nonlocal symmetry, darboux transformation and soliton-cnoidal wave interaction solution for the shallow water wave equation. J Math Anal Appl 2018;460:987–1003.
[45] Huang LL, Yue YF, Chen Y. Localized waves and interaction solutions to a (3+1)-dimensional generalized KP equation. Comput Math Appl 2018;76:831–44.
[46] Yue YF, Huang LL, Chen Y. Localized waves and interaction solutions to an extended (3+1)-dimensional jimbo-miwa equation. Appl Math Lett 2019;89:70–7.
[47] Huang LL, Chen Y. Localized excitations and interactional solutions for the re duce d maxwell-bloch equations. Commun Nonlinear Sci Numer Simulat 2019;67:237–52.
[48] Su JJ, Gao YT. Bilinear forms and solitons for a generalized sixth-order nonlinear schrödinger equation in an optical fiber. Eur Phys J Plus 2017;132:53.
[49] Sun WR. Breather-to-soliton transitions and nonlinear wave interactions for the nonlinear schrödinger equation with the sextic operators in optical fibers. Ann Phys 2017;529:1600227.
[50] Lan ZZ, Guo BL. Conservation laws, modulation instability and solitons interactions for a nonlinear schrödinger equation with the sextic operators in an optical fiber. Opt Quantum Electron 2018;50:340.
[51] Akhmediev N., Ankiewicz A.. Solitons, nonlinear pulses and beams. Chapman and Hall, London. 1997.
[52] Ankiewicz A, Soto-Crespo JM, Akhmediev N. Rogue waves and rational solutions of the hirota equation. Phys Rev E 2010;81:046602.
[53] Ankiewicz A, Akhmediev N. Higher-order integrable evolution equation and its soliton solutions. Phys Lett A 2014;378:358–61.
[54] Akhmediev N, Ankiewicz A, Soto-Crespo JM, Dudley JM. Rogue wave early warning through spectral measurements. Phys Lett A 2011;375:541–4.
[55] Akhmediev N, Soto-Crespo JM, Devine N, Hoffmann NP. Rogue wave spectra of the sasa-satsuma equation. Physica D 2015;294:37–42.
[56] Bayindir C. Rogue wave spectra of the kundu-eckhaus equation. Phys Rev E 2016;93:062215.
[57] Wang X, Liu C, Wang L. Rogue waves and w-shaped solitons in the multiple self-induced transparency system. Chaos 2017;27:093106.
[58] Wang X, Liu C. W-Shaped soliton complexes and rogue-wave pattern transitions for the AB system. Superlattices Microstruct 2017;107:299–309.
[59] Droques M, Barviau B, Kudlinski A, Taki M, Boucon A, Sylvestre T, et al. Symmetry-breaking dynamics of the modulational instability spectrum. Opt Lett 2011;36:1359–61.
[60] Solli DR, Herink G, Jalali B, Ropers C. Fluctuations and correlations in modulation instability. Nat Photonics 2012;6:463–8.
[61] Zhao LC, Ling LM. Quantitative relations between modulational instability and several well-known nonlinear excitations. J Opt Soc Amer B 2016;33:850–6.
[62] Liu C, Yang ZY, Zhao LC, Duan L, Yang GY, Yang WL. Symmetric and asymmetric optical multipeak solitons on a continuous wave background in the femtosecond regime. Phys Rev E 2016;94:042221.
[63] Duan L, Zhao LC, Xu WH, Liu C, Yang ZY, Yang WL. Soliton excitations on a continuous-wave background in the modulational instability regime with fourth-order effects. Phys Rev E 2017;95:042212.
[64] Yang YQ, Yan ZY, Malomed BA. Rogue waves, rational solitons, and modulational instability in an integrable fifth-order nonlinear schrödinger equation. Chaos 2015;25:103112.
[65] Li P, Wang L, Kong LQ, Wang X, Xie ZY. Nonlinear waves in the modulation instability regime for the fifth-order nonlinear schrödinger equation. Appl Math Lett 2018;85:110–17.